Optimization of Epsilon-Near-Zero Multilayers for Near-Perfect Light Absorption Using an Enhanced Genetic Algorithm

Yuqing Wang, *Student Member, IEEE*, Jiaye Wu, *Student Member, IEEE*, Zimiao Wang, *Student Member, IEEE*, Chenxingyu Huang, *Student Member, IEEE*, H. Y. Fu, *Senior Member, IEEE*, and Qian Li, *Senior Member, IEEE*

***Abstract*—Using epsilon-near-zero (ENZ) subwavelength optical multilayer materials with simple structure and thin total thickness to achieve target characteristics is extremely important and beneficial for the realization of on-chip integration and large-scale application of optical devices. Combining with the enhanced genetic algorithm (EGA), this work breaks the limitation of the periodicity of traditional ENZ multilayer structures, and investigates the aperiodic ENZ transparent conducting oxide (TCO)-dielectric multilayer structures. It is realized that under the given conditions, an optimal structure can possess a maximum peak absorption and the broadest absorption bandwidth near the communication wavelength. In the 6-layer structure with a total thickness of 600 nm studied in this work, EGA can optimize the peak absorption from 0.91 to 0.95. Additionally, the absorption bandwidth is optimized from 120 nm to 227 nm, which is enhanced more than 180%. The absorption performance of this optimized structure is comparable to that of a more complex structure with the same total thickness but more layers, or a structure with the same number of layers but a larger total thickness. Conclusively, the proposed EGA optimization method can simplify the structure of the multilayer system, reduce the total thickness of the required ENZ material, and thus greatly simplify the production process and reduce the production cost.**

***Index Terms*—Enhanced genetic algorithm, ENZ material, indium tin oxide, light absorption, multilayer.**

I. Introduction

EPSILON-near-zero (ENZ) materials are a kind of near-zero-index materials [1]. These ENZ materials possess many unique characteristics, such as strong field enhancement [2]–[4], constant phase transmission [5], [6], tunneling through distorted channels [7], [8] and etc. ENZ photonics has attracted extensive attention in recent years, which is considered as a new platform for integrating photonic and nanophotonic devices [9]–[12]. In combination with ENZ materials, a variety of optical metamaterials and devices with different functions have been designed based on hollow waveguide structures [13], [14], grating structures [10], [15], [16], multilayer structures [17], [18] and complex hybrid structures [19], [20].

Multilayer structure is one of the most common methods to realize an effective ENZ point [17]. It follows the effective medium theory (EMT) [21] to achieve near-zero permittivity with metal-dielectric or TCO-dielectric alternating structures. ENZ multilayer structures have many advantages, such as the ability to adjust the ENZ wavelength by changing the type of materials or changing the thickness proportion of different materials [17]. Through the designing of the multilayer structures, the enhancement of nonlinear optical effects [22], controlling of plasma resonance [20], modulation of material absorption [23]–[26], and ultra-fast optical tuning [27] have been realized. Among them, the absorption characteristics of materials can be applied in solar energy collection [28], heat emitters in thermo-photocells [29], photocatalysis [30] and etc. ENZ multilayer takes advantage of the intrinsic absorption of the ENZ material near the ENZ point to increase the loss of light transmission, which is strengthened in the structure through the localized multimode resonance between the layers, thus helps to achieve a near-perfect absorption. Its applications include the design of absorbers and electro-optical modulators, filters and other applications of the communication systems.

Most of the studies on the absorption performance of ENZ multilayers are based on periodic structures [17], [18], [22]. A metal-dielectric pair is taken as a period and its optical absorption performance is improved by adjusting the total thickness or the number of multilayer periods. The absorption performance can also be enhanced by adding grating structure on the metasurface of the multilayer [10]. However, increasing the total thickness of the multilayer increases the volume and the production cost, which limits the integration level; and increasing the number of multilayer periods and introducing gratings increase the manufacturing difficulties. From the fabrication perspective, the structure of the multilayer needs to be properly optimized. In previous works, the optimal periodic multilayer structures are obtained by fixing one variable and exhaustively

Manuscript received August 1, 2021; revised September 5, 2021; accepted September 14, 2021. Date of publication September 21, 2021; date of current version October 15, 2021. This work was supported in part by Guangdong Basic and Applied Basic Research Foundation under Grants 2021A1515012176 and 2021A1515011450, in part by Shenzhen Fundamental Research Program under Grant GXWD20201231165807007-20200827130534001, and in part by the Youth Science and Technology Innovation Talent of Guangdong Province under Grant 2019TQ05X227. *(Corresponding author: Qian Li.)*

Yuqing Wang, Jiaye Wu, Zimiao Wang, Chenxingyu Huang, and Qian Li are with the School of Electronic and Computer Engineering, Peking University, Shenzhen 518055, China (e-mail: wangyuqing@stu.pku.edu.cn; jiayewu@pku.edu.cn; zimiaow@stu.pku.edu.cn; hcxy@stu.pku.edu.cn; liqian@pkusz.edu.cn).

H. Y. Fu is with the Tsinghua Shenzhen International Graduate School, Tsinghua University, Shenzhen 518055, China (e-mail: hyfu@sz.tsinghua.edu.cn).

Digital Object Identifier 10.1109/JPHOT.2021.3113924

enumerating others [22], and the multilayer structure is effectively optimized to an extent. However, manual parameter search is a time-consuming and laborious process, and optimization method is proven to be useful [31]. It is reported that conventional genetic algorithm (GA) has been implemented to design the optical structures (e.g., [32]–[34]), modified GA with more efficiency and faster speed has not been introduced to the realm of TCO-dielectric alternating ENZ multilayers.

In this work, we propose an EGA method to greatly improve the absorption characteristics of ENZ multilayers. Firstly, we investigate the case where the thickness of each pair of TCO-dielectric is optimized with a fixed total thickness. The optimized structure breaks the limitation of the periodic multilayer structure design, realizes the equivalent absorption effect of a more complex structure with fewer layers in terms of peak absorption and absorption bandwidth. In the 6-layer structure with a total thickness of 600 nm, EGA can optimize the peak absorption from 0.91 to 0.95. Additionally, the absorption bandwidth is optimized from 120 nm to 227 nm, which is enhanced more than 1.8 times. The optimal absorption effect of fixed numbers of layers with different total thicknesses is then studied. The findings of these two aspects are beneficial to give full play to the absorption performance of the limited material and simplify the process of design and fabrication.

The framework of this work is as follows. The absorption mechanisms of ENZ multilayer structures are discussed in Section II. The design process and absorption optimization utilizing EGA is shown in Section III. The results of the absorption performance optimization of ENZ multilayers with a fixed total thickness are shown in Section IV. The optimal absorption performance can be achieved by a fixed number of layers of different thicknesses, which is discussed and explored in Section V. Section VI is the conclusion of this paper.

II. Absorption Mechanisms of ENZ Multilayers

It has been reported that there are many material combinations of ENZ multilayer structures [35], such as Au and CdO [18], Ag and SiN [36], Ag and indium tin oxide (ITO) [37], Ag and TiO_2 [15], Ag and SiO_2 [38], ITO and SiO_2 [23], AZO of different doping levels [39]. Different combinations of materials have different ENZ wavelengths and different ENZ-related properties. Among them, ITO is the most studied photonic medium in TCOs, which is suitable for integration. The ENZ wavelength of ITO can be tuned by adjusting the free carrier concentration [40]. Additionally, ITO has the advantages of CMOS compatibility and ultra-fast response [41]. Studies have shown that the stacked structure of layers composed of alternating ENZ material and dielectric can enhance the refraction, reflectance or absorption of the multilayer systems [22], for instance, the combination of ITO and SiO_2 has good absorption characteristics [23].

Therefore, an alternating structure of ITO and SiO_2 is selected for the study in this work, as shown in Fig. 1(a). A layer of titanium nitride (TiN) film of appropriate thickness is placed below the alternating ENZ multilayer structure. TiN films are often used as the light-absorbing material for solar cells. In this case, it is used to increase absorption and isolate the effect of the substrate material on the optical properties of the

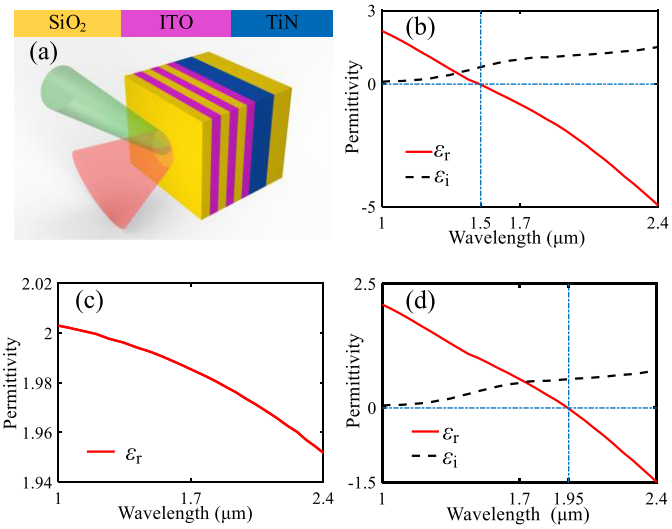

Fig. 1. (a) 3D schematic overview of an optical 6 alternating layers of ITO and SiO_2 structure with the incident and the reflected light, and with a layer of TiN at the bottom, which is deposited on a SiO_2 substrate. (b) The variation of the real (solid red line) and imaginary parts (dotted black line) of the complex permittivity of ITO, as a function of the wavelength. Re(ε) vanishes at $\lambda_{\mathrm{ENZ}} =$ 1500 nm. (c) The variation of the real part (solid red line) of the permittivity of SiO_2, as a function of the wavelength. (d) The variation of the real (solid red line) and imaginary parts (dotted black line) of the complex permittivity of the ITO-SiO_2 alternating structure, as a function of the wavelength. Re(ε) vanishes at $\lambda_{\mathrm{ENZ}} = 1950$ nm.

upper multilayer structures. Through the simulations of various thickness values, 0.3 μm is selected here. This thickness value has a better effect on the enhancement of absorption and will not increase the volume of the structure too much. The whole structure is placed on a commonly used SiO_2 substrate, which is experimentally feasible. In addition to the high peak absorption, this combination can also achieve a broad absorption bandwidth. It is promising to optimize the absorption characteristics of this alternating structure.

The permittivities of ITO and SiO_2 used in this structure are acquired from the experimental measurements in the reference [23], as shown in Figs. 1(b) and 1(c). These two materials are not permeable to each other, therefore, they can be alternately sputtered together. The ENZ wavelength of ITO is around 1500 nm, which is close to the communication wavelength. In this study, we set the total thickness of the two materials to be the same, and the proportion of the two materials in the whole multilayer system is the same. We can use EMT to calculate the effective permittivity of such alternating stacked structures. It is clear that the multilayer structure is an anisotropic material. The permittivity can be well described by the commonly used Maxwell-Garnett equation [21]:

$$\varepsilon_{||} = \frac{\varepsilon_{\mathrm{d}} L_{\mathrm{d}} + \varepsilon_{\mathrm{m}} L_{\mathrm{m}}}{L_{\mathrm{d}} + L_{\mathrm{m}}}, \tag{1}$$

in which L is the thickness of the material, and the subscripts d and m represent the dielectric material and the metal-like material, respectively. Through the EMT calculation, the ENZ wavelength of the whole multilayer system is 1950 nm, which is close to new communication window of 2 μm, as shown in Fig. 1(d).

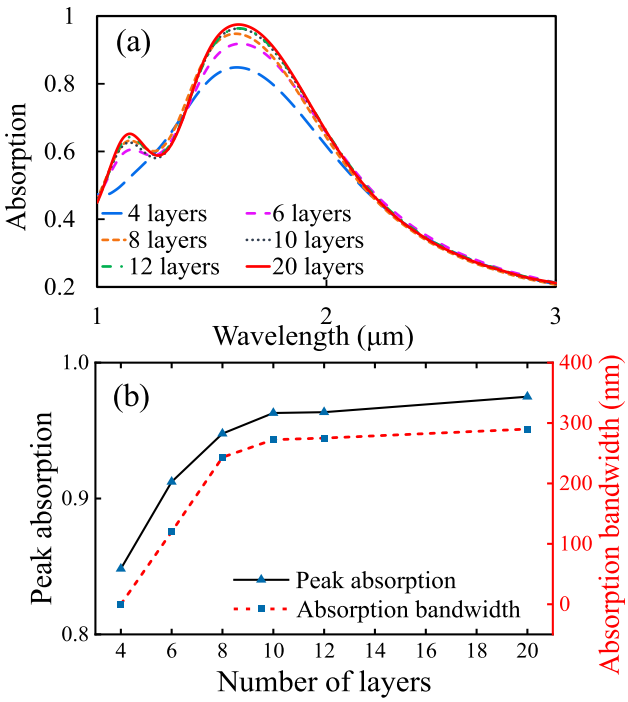

Fig. 2. (a) Absorption curves of different numbers of layers at different wavelengths with a total thickness of 600 nm. (b) Peak absorption values (solid black line) and absorption bandwidths (dotted red line) corresponding to different numbers of layers.

In order to study the absorption mechanisms of the ENZ multilayers, the material is divided into different numbers of layers of the same thickness in the condition of a fixed total thickness. For the convenience of calculation and without loss of generality, we take the total thickness of 600 nm as an example first. Then the effect of different numbers of layers on the overall absorption of the material is studied. The absorption of different layers at different wavelengths is calculated by the finite-difference time-domain (FDTD) method (with the commercial Lumerical FDTD software), as shown in Fig. 2(a). As can be seen from the figure, when the total thickness is a fixed value, the more layers the material is divided into, the greater the peak absorption values and the broader the absorption bandwidths are. Here we define the absorption band as the wavelength range corresponding to an absorption rate greater than 0.9. The peak absorption values and absorption bandwidths corresponding to different layers are shown in Fig. 2(b). It can be found that the peak absorption appears at the wavelength that maximizes the ratio of $|\mathrm{Im}(\varepsilon_{\mathrm{ITO}})|/|\mathrm{Re}(\varepsilon_{\mathrm{ITO}})|^2$, near the communication wavelength, and it may be caused by the plasmon resonance of ITO near the ENZ point [42]. With the increase of the number of layers, the thickness of each layer decreases, and the whole multilayer structure shows better absorption effect due to the enhanced light scattering and the enhanced light localization caused by the multimode resonance effect [43], [44]. Therefore, increasing the number of layers is beneficial to improve the absorption bandwidth. However, too many layers will increase the complexity of the production process and also lead to the accumulation of unevenness from each layer. Therefore, we need to find an optimization method to achieve greater absorption with fewer layers at a fixed total thickness of the material.

III. Absorption Characteristics Improvement Based on EGA

The proposed optimization algorithms are developed to solve problems involving multiple variables. GA is a commonly used evolutionary algorithm for optimization, and it was first proposed in the 1970s [45]. It is a computational model inspired by the biological evolution process which optimizes parameters by the emulation of natural selection and genetic mechanism (i.e., chromosome crossover and gene mutation). When solving more complex combinatorial optimization problems, compared with traditional algorithms, GA can usually obtain better results faster. GA has been widely used in combinatorial optimization [46], machine learning [47], signal processing [48], adaptive controlling [49], etc. In recent years, GA is also used in photonics [50]–[52].

In this study, we combine the basic principles of GA and implement additional improvements, thus the EGA. Compared with the conventional GA, EGA has great advantages in searching ability and convergence ability. The calculation process of EGA is mainly divided into three stages, which will be described in detail as we introduce the fitness function and the transfer matrix method (TMM), which are all essential concepts in our proposed EGA.

First, a fitness function should be determined according to the design objective. The fitness function is the evaluation criterion for all variables. Here, the design goal is to achieve near-perfect absorption and broad absorption bandwidth (as defined above, corresponds to the wavelength range where absorption is larger than 0.9). In this study, the fitness function is defined as the absorption bandwidth. With the broadening of absorption bandwidth, the peak value will also be improved accordingly. Therefore, the fitness function is set to be related to both peak absorption and bandwidth, which can evaluate the total absorption performance of the multilayer structures. The larger the fitness function value of the multilayer structure is, the better the absorption effect is obtained.

According to the conventional GA process, 80 individuals are randomly generated within a given thickness range firstly. Each individual represents the thickness values of each layer of a set of multilayer system to form the initial population. When the population size is small, the algorithm has a limited ability to search for information and it is difficult to approach or reach the optimal solution. When the population size is large, the algorithm has sufficient information and it is easier to approach or reach the optimal solution. However, if the population size is too large, the calculation time of circulation will be greatly increased. Therefore, the proper selection of the population size is the premise for the algorithm to obtain the optimal solution quickly. The fitness value is then calculated by using the TMM to calculate the absorption rate for each individual (each multilayer structure). The calculation of TMM is based on the characteristic

matrix of multilayer systems [53]:

$$\begin{bmatrix} B \\ C \end{bmatrix} = \left\{ \prod_{j=1}^{K} \begin{bmatrix} \cos\delta_j & \mathrm{i}\sin\delta_j/\eta_j \\ \mathrm{i}\eta_j \sin\delta_j & \cos\delta_j \end{bmatrix} \right\} \begin{bmatrix} 1 \\ \eta_s \end{bmatrix}, \tag{2}$$

where η_s, η_j, and δ_j are the admittance of the substrate, the admittance in the *j*th medium and the phase thickness in the *j*th medium, respectively. The parameters *B* and *C* are widely-used specific values in the characteristic matrix for film systems [53] and they can be used to calculate the transmission, reflection and absorption of the film system. From this matrix, the reflection of the film system can be calculated as:

$$R = \left(\frac{\eta_0 B - C}{\eta_0 B + C}\right)\left(\frac{\eta_0 B - C}{\eta_0 B + C}\right)^*, \tag{3}$$

where η_0 is the admittance of the incident medium. And the transmission of the film system can be calculated as:

$$T = (1-R)\frac{\eta_{K+1}}{\mathrm{Re}\,(BC^*)} = \frac{4\eta_0\eta_{K+1}}{(\eta_0 B + C)\,(\eta_0 B + C)^*} \tag{4}$$

Combined with the above formulas, the absorption (*A*) can be calculated by *A* = 1-*T*-*R*. The thickness of each layer affects the value of the phase thickness, which in turn affects the absorption. Different individuals have different absorption effects. Of course, there will be a best fitness function value in the initial population. Also, the average fitness function value can be calculated. This is the first stage of EGA, which is called the initialization stage.

The process of generating new individuals runs through the second and the third stages of EGA. Selection, crossover, and mutation occur in both these two stages. In this study, 10 new individuals are set to be generated in each generation. The maximum population size is set to be 280, and it takes 20 generations to reach the maximum population. This stage is the second stage of EGA. After the maximum population size of 280 is reached, the effect of generating 10 new individuals in each generation is no longer to increase the population size, but to replace the 10 individuals with the lowest fitness values in the population, thus maintaining the population size. This stage is the third stage of EGA. Conventional GA generates individuals equal to the population size and replaces all the individuals of the previous generation. This EGA selects some excellent individuals as parents, generates only 10 new individuals, and replaces the worst individuals of the previous generation according to the principle of replacing the worst. So the population can evolve more stably towards a higher fitness function value in this process, which also improves the convergence ability of the population to a certain extent. And the updated population is sorted according to the fitness function values of individuals, so as to make the individuals with high fitness more likely to be selected by the roulette method. In this work, we set the number of iterations to be 300, which is to produce 300 new generations of individuals. The value 300 is chosen because after 300 generations, the fitness function converges to a fixed value and it takes more time to generate more generations. The setting of this value takes into account the time consumption of the circulation and the rate at which the optimal value converges.

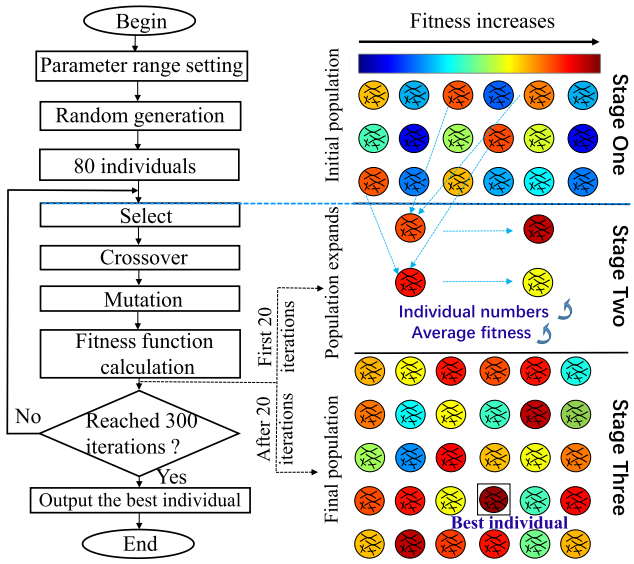

Fig. 3. Diagram of the operation of EGA. The flow chart on the left corresponds to the stages in the schematic diagram on the right. A circle represents an individual, each of which contains chromosomes. The closer the color of the circle to the dark red, the greater the fitness function value.

After 300 generations of new individuals are generated, the thickness of the films corresponding to the individual with the greatest fitness is selected as the structure of the ENZ multilayer with the best absorption performance after optimization. The entire EGA optimization process is shown in Fig 3.

Specifically, the second and third stages involve crossover and mutation processes. In this work, the mechanism by which the individuals are produced is that in each generation 30 individuals are chosen as parents. The 30 individuals are composed of 10 individuals with best fitness function values in the current population and 20 individuals selected by the conventional roulette method. This mechanism ensures that the optimal 10 individuals will not be disturbed by the randomness of the roulette selection process, and can definitely participate in the crossover and mutation process as the parents, which improves the global convergence ability. The other 20 individuals randomly selected by roulette provide diversity for the parent samples and prevent GA from falling into local convergence. This elite preservation strategy enables the best individuals in the current population to directly influence the next generation, making the population develop faster towards a higher average fitness function value, and reducing the iterations required for convergence.

The method of simulated binary crossover (SBX) is adopted in the crossover process, which is more accurate than the conventional binary crossover process in GA and the coding complexity is reduced [54]. And the crossover operator is:

$$\hat{X} = \begin{bmatrix} 0.5(1+\sigma) & 0.5(1-\sigma) \\ 0.5(1-\sigma) & 0.5(1+\sigma) \end{bmatrix}, \tag{5}$$

$$\sigma = \begin{cases} (2u)^{1/(n+1)}, u \le 0.5 \\ (2-2u)^{-1/(n+1)}, u > 0.5 \end{cases}, \; u \in [0,1), \tag{6}$$

where the transmission factor σ is defined as the ratio of the difference between the new individuals and the parents. Equation (6) is used to fit the binary code process by a uniform distribution random number u. The spread factor n is used to determine the similarities between new individuals and parents. A large n gives higher probability for generating the new individuals near the parents. The crossover rate is 0.8. Among the 30 individuals selected as parents in each generation, two individuals are randomly selected as parents. If the random number generated at this moment is less than the crossover rate, crossover will occur, and new individuals will be generated. Conversely, there is no crossover and no new individual is produced. The crossover process of each generation ends after 10 individuals have been generated.

The mutation process follows the crossover process. On the one hand, mutation can improve the local searching ability of EGA; and on the other hand, it can maintain the diversity of population and prevent the phenomenon of premature. There are two ways to enhance the conventional mutation process, which can be divided into adaptive mutation and non-uniform mutation according to different principles. The mutation amplitude of adaptive mutation is related to the fitness function value, that is, when the current fitness function value differs greatly from the target fitness function value, the mutation amplitude will be large. Otherwise, the mutation amplitude will be small. The mutation amplitude of non-uniform mutation decreases with the increase of iterations. The non-uniform mutation process allows a large mutation range in the early stage of EGA, and the mutation range will be gradually shrunk to the approximate solution along with the continuous iterations. In order to prevent local convergence of fitness function values, this non-uniform mutation is chosen in this work [55], which is an improvement over GA. The mutation process can be described as:

$$I'_{\mathrm{k}} = I_{\mathrm{k}} + \Delta\left(t, I_{\mathrm{k}}^{\max} - I_{\mathrm{k}}\right) \text{ or } I'_{\mathrm{k}} = I_{\mathrm{k}} - \Delta\left(t, I_{\mathrm{k}} - I_{\mathrm{k}}^{\min}\right), \tag{7}$$

where I_{k} respectively represents the thickness values of different layers, and I'_{k} represents the corresponding mutated thickness values (k = 1,2,3 …). The terms with a superscript are the maximum and minimum values of I_{k}, respectively. And the amount of mutation can be defined as:

$$\Delta(t, m) = m \cdot \left(1 - u^{(1-t/T)^h}\right), \tag{8}$$

where t is the current iteration and T is the total iterations of EGA. And m is the difference between the thickness of a current layer and the upper or lower limit. And h is the term that determines the property of non-uniform, which is generally distributed between 2 to 5. Ten new individuals are randomly selected to undergo the mutation process. The mutation rate is 0.3. If the random number generated at this moment is less than 0.3, the mutation will occur, that is, the thicknesses of all layers will change. Conversely, there will be no mutation. If no mutation occurs, individuals still retain the thicknesses after the crossover process.

To summarize, the conventional GA has been enhanced by using elite preservation strategy, SBX and non-uniform mutation processes. Thus the processes of selection, crossover, and mutation are all optimized. For the 6-layer structure in this paper, the whole calculation process of EGA combined with the verification process of FDTD takes less than 10 minutes on a 2.9 GHz dual-core Intel Core i5 processor. However, if the conventional GA is used, it takes tens of minutes to calculate, and the results obtained each time are not always the optimal solution, which may converge to different values. This may require multiple validations using FDTD, which can be time-consuming.

IV. EGA Optimization of ENZ Multilayers With a Fixed Total Thickness

In the settings of optimization program and the verification of optimization results, we find that a pair of alternating structure of ITO and SiO_2 with the same thickness have better absorption effect than those with different thickness. This is caused by the localized resonance and coupling effect of the alternating structure of ITO and SiO_2. Therefore, we set the thickness of ITO and SiO_2 in a pair to be the same in this optimization process. The multilayers with the thickness of several hundred nanometers are used in most researches, and the thickness of 600 nm can be divided into many combinations of layers with the same thickness. Therefore, in this study, a multilayer structure with a total thickness of 600 nm is taken as an example to illustrate the optimization process.

The absorption characteristics of 4, 6, 8 and 10 layers of the 600-nm material have been studied in this work. Among them, the improvement for the 6-layer structure is prominent. Here, the 6-layer structure is taken as an example for detailed introduction. According to the established procedure, the fitness function value of the 6-layer structure is determined by the three thickness values adding up to 300 nm. We can regard these three thicknesses as variables on the three axes x, y, and z. The optimization process is regarded as the process of finding a point with the best fitness function value in a three-dimensional space, as vividly illustrated in the stereoscopic diagram Fig. 4(a). Similarly, the process of optimizing a 10-layer structure can be viewed as to find a point in a hypothetical five-dimensional space where the fitness function value is maximized.

In the optimization process of EGA, the best fitness function value and average fitness function value of the 6-layer multilayer structure are gradually improved, as shown in Fig. 4(b). Finally, it plateaus at a stable value, which is the optimal ENZ multilayer structure under the given conditions. Before optimization, the 6-layer multilayer structure is alternately composed by 6 layers of 100-nm thick ITO and 100-nm thick SiO_2. The optimized structure is no longer periodic and is shown in Fig. 5(a). The upper layer of multilayer structure is thinner and the bottom layer is thicker. This means that different pairs of alternating structures are different in their ability to absorb light during the transmission process. For the 6-layer structure, the upper layers have a greater effect on the local plasmon resonance. Although the values of thickness are not the same in the stochastic process, the crossover, and mutation process, they all converge to the same set of thickness values after enough generations. That indicates that this structure is the optimal configuration in the current conditions. The structures before and after optimization are then simulated by FDTD to verify the improved absorption

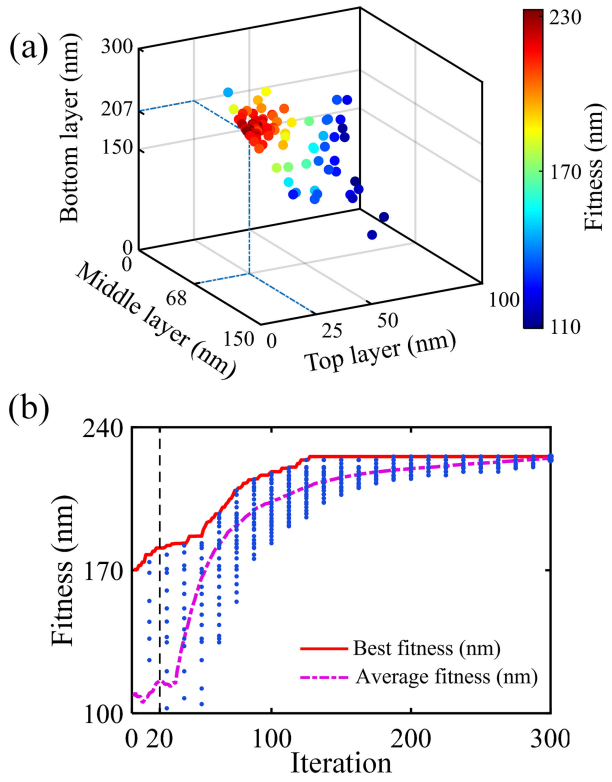

Fig. 4. (a) Scatter diagram of 280 individuals generated by EGA for a 6-layer structure. The color of the points shows the fitness function values of each individual. Warmer color points have bigger fitness function values and the optimal individual is represented in the figure as the red point with the darkest color sited in the coordinates of the three optimized parameters. (b) The evolution of the maximum (solid red line) and average (dotted pink line) fitness function values with the increase of the number of iterations. The blue dots represent the fitness function values of different individuals in the population.

performance. Fig. 5(b) is the comparison of the absorption curves before and after optimization of the 6-layer multilayer structures. The peak absorption of the unoptimized 6-layer structure is 0.91, with an absorption bandwidth of 120 nm. The peak absorption of the optimized 6-layer structure is 0.95, with a bandwidth of 227 nm. The peak absorption and absorption bandwidth are improved remarkably.

The discussion above is based on the assumption that the permittivity of ITO with different thickness remains unchanged within a certain range. We set the upper and lower limits of thickness variation in the EGA process, and the difference between the maximum thickness value and the minimum thickness value in each structure is no more than one order of magnitude. The minimum thickness is set to be no less than 20 nm, so it's almost impervious to dead-layer phenomenon [56]. The dependency of ITO permittivity on the film thickness and its impact on the absorption is also studied. According to the relationship between the permittivity and thickness of ITO in the reference [56], FDTD is used to simulate the optimized 6-layer structure, as shown in Fig. 6. It is proved that the peak absorption and the absorption bandwidth are further optimized after considering the influence of ITO thickness.

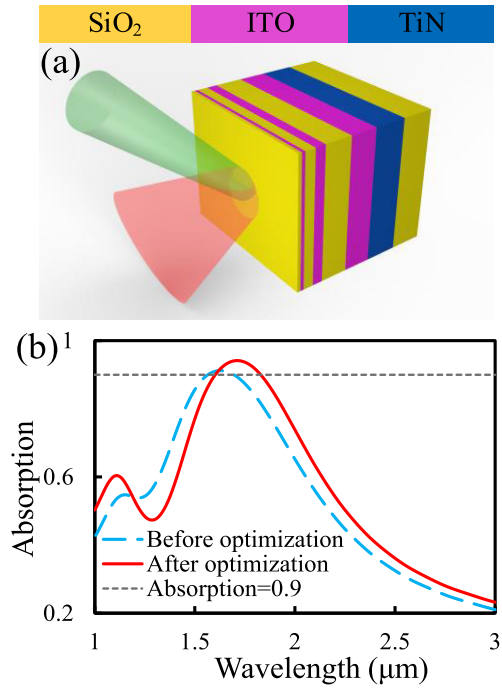

Fig. 5. (a) 3D schematic overview of the optimized aperiodic 6-layer structure with the incident and the reflected light. (b) Absorption performance before optimization (dotted blue line) and after optimization (solid red line) of the 6-layer multilayer structures.

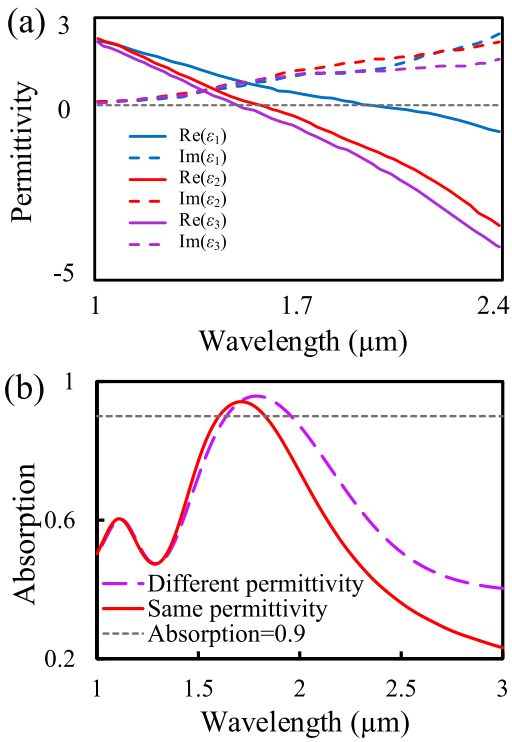

Fig. 6. (a) The variation of the real (solid line) and imaginary parts (dotted line) of the complex permittivity of ITO, as a function of the wavelength. The blue lines are for the top layer, the red lines are for the middle layer and the purple lines are for the bottom layer of the optimized 6-layer structure. (b) Absorption performance for the optimized 6-layer structure with the same permittivity for each layer and different permittivity for each layer, respectively.

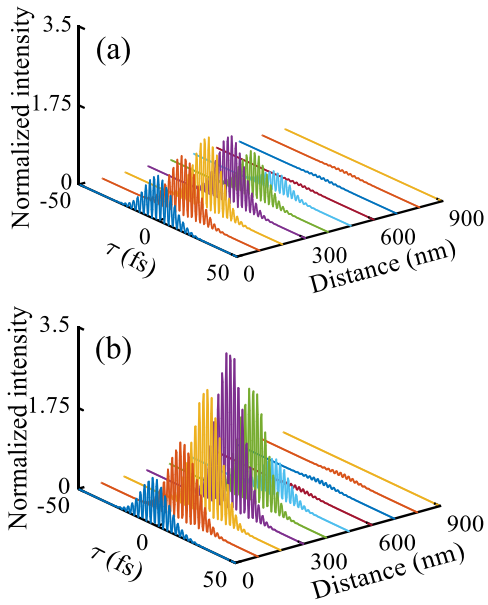

Fig. 7. The evolution of the intensity of the EM field for the 6-layer structures (a) before optimization and (b) after optimization in temporal domain, calculated by FDTD. In (a) and (b), 0 nm corresponds to the upper surface of the multilayer and 900 nm to the lower surface of the TiN substrate.

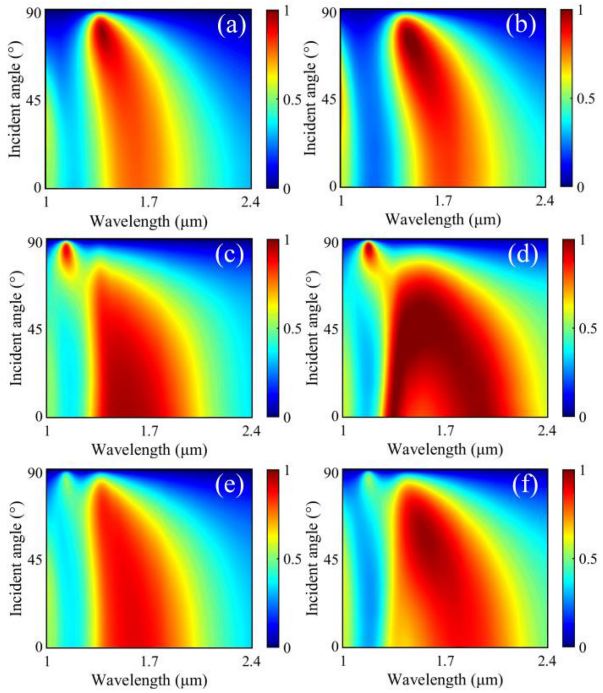

Fig. 8. Calculated optical absorption versus wavelength ranging from 1 μm to 2.4 μm and incident angle ranging from 0° to 90° for (a) TE wave, (c) TM wave and (e) circular-polarized wave of the unoptimized 6-layer structure, and (b) TE wave, (d) TM wave and (f) circular-polarized wave of the optimized 6-layer structure.

To better explain the mechanism of the improvement in absorption performance, an ultrashort 20-fs pulse is incident into the multilayer structures to observe the distribution of the electromagnetic (EM) energy. The results of the 6-layer multilayer structures before and after optimization are shown in Figs. 7(a) and 7(b). It can be seen that there is a large degree of field enhancement in the upper part of the multilayer after optimization compared with that before optimization. After optimization, the field enhancement effect is more than doubled. The increase in absorption is probably due to a reduction in the reflected power as a consequence of reducing the mismatch between the structure and free space.

Different kinds of waves behave differently in the medium, and different kinds of waves will have different absorption effects. In order to further explore the degree of improvement of EGA on absorption performance, transverse electric (TE) wave, transverse magnetic (TM) wave and circular-polarized wave with incident angle range from 0° to 90° are studied in the 6-layer structures before and after optimization. TMM is still used to calculate the absorption rate of multilayers. It is worth noting that the optical admittances of the TE and TM waves are no longer degenerated when the EM waves are of oblique incidence, with $\eta_j = n_j \cos\theta_j$ for TE and $\eta_j = n_j / \cos\theta_j$ for TM based on Eqs. (2) to (4). The circular-polarized wave is calculated by taking the average of TE and TM waves [53]. The simulation results are shown in Fig. 8. It can be seen from the figures that the absorption effects of the optimized structure on these three kinds of waves are all better than those of the unoptimized structure. Obviously, the case also holds true for waves with different elliptical polarizations. Moreover, the optimization is robust against the variation of the incident angle, showing a relatively uniform absorption band across different angles. The absorption bands of TM wave are wider than that of TE wave. This phenomenon is consistent with the fact that the absorption property (including the peak value and the defined bandwidth) for TM wave is better than that for TE wave in most materials [57]–[59]. For circular-polarized wave, the optimized structure also shows better absorption near the communication wavelength, where the color level is closer to dark red.

In further simulations, it is found that due to the different thickness values of different pairs of ITO and SiO_2 alternating structure, the spectral location of the peak values will also be different. The optimal 6-layer structure is thicker in the lower layer, and the peak absorption has an obvious red shift. Several groups of structures with thicker upper layer and thinner lower layer are simulated. It can be observed that the peak value has an obvious blue shift, which is due to the effect of the thickness on the plasmon resonance wavelength. According to this phenomenon, we can use the multilayer structures to manipulate the wavelength where the maximum absorption occurs.

Additionally, this optimization process is applied to improve the absorption characteristics of 4, 6, 8 and 10 layers with a total thickness of 600 nm. The absorption curves before and after optimization are shown in Fig. 9(a), and the peak absorption values and bandwidths before and after optimization of different layers are shown in Fig. 9(b). As the number of layers increases, the optimization margin of peak value and bandwidth gradually decreases. When the number of layers reaches 10, the margin of optimization is already small. That is to say, when the number

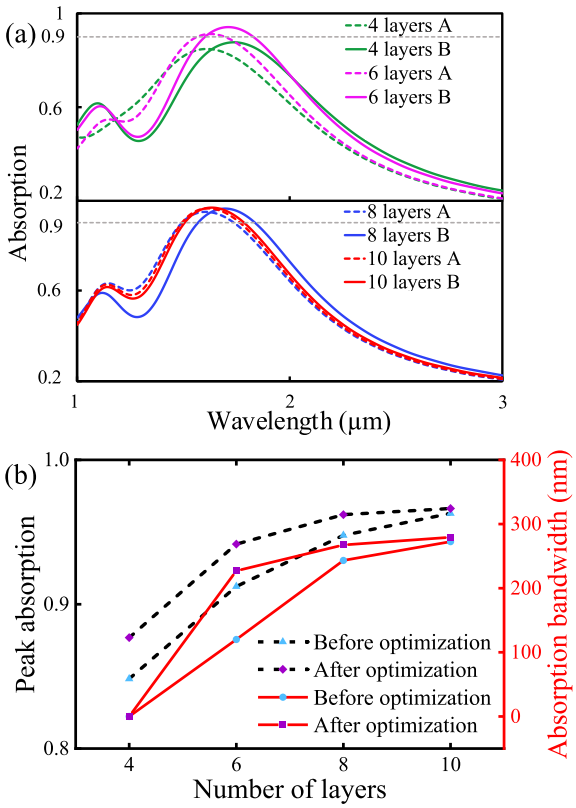

Fig. 9. (a) The absorption characteristics of 4, 6, 8, and 10 layers before (labeled A) and after (labeled B) optimization with a total thickness of 600 nm. (b) Peak absorption values (dotted black line) and absorption bandwidths (solid red line) before and after optimization corresponding to different numbers of layers.

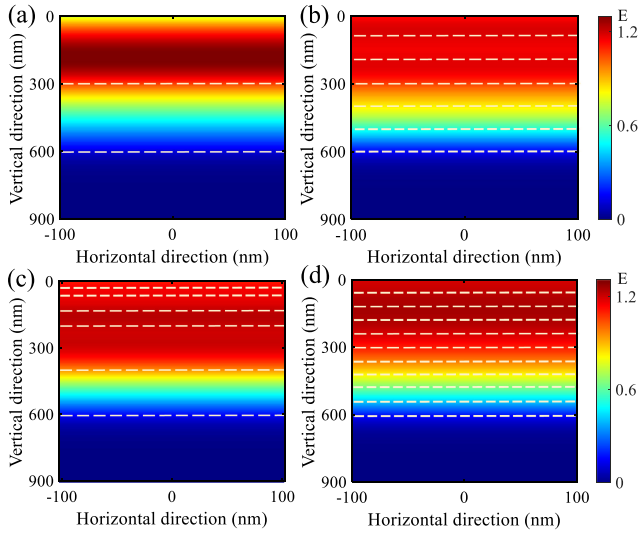

Fig. 10. The field distribution of (a) 2-layer, (b) unoptimized 6-layer, (c) optimized 6-layer, and (d) unoptimized 10-layer structures at the peak absorption wavelength, respectively. The x coordinate represents the transverse simulation range of multilayer structures. For the y coordinate of the figures, 0 nm corresponds to the upper surface of the multilayer and 900 nm to the lower surface of TiN. The dashed lines correspond to the boundaries of each layer in these structures.

of layers is large, the increase of the number of layers plays a major role in the influence of absorption. Moreover, the absorption performance of the material with a fixed thickness has its physical limit. When the number of layers reaches a certain value, it is useless to increase the absorption by increasing the number of layers, even when the EGA method is used. It can also be seen from the figure that, the absorption performance of the 6-layer structure has been significantly improved, which can almost achieve perfect absorption. It is worth noting that the peak absorption of the unoptimized 8-layer periodic structure is 0.95, and the bandwidth is 240 nm. The optimized aperiodic 6-layer structure can achieve the absorption effect of the periodic 8-layer structure with the same thickness. Similarly, the peak absorption and absorption bandwidth of the optimized 8 layers have exceeded that of the 10 layers. If fewer layers are able to achieve the same effect, the number of sputtering processes in the fabrication can be effectively reduced, which also reduces the accumulative effect of the total unevenness of the thin films from the lower layers to the upper ones.

Fig. 10 shows the field distribution at the cross-sections of the 2-layer, unoptimized 6-layer, optimized 6-layer and unoptimized 10-layer structures at the peak absorption wavelength. The attenuation situation of the EM wave in those structures can be clearly compared. It can be seen that the field is localized in some upper layers of media. The 2-layer structure has a poor light restriction effect, as shown in Fig. 10(a). As shown in Figs. 10(b) and 10(c), the red region of the 6-layer multilayer structure after optimization is wider than that before optimization. The localization effect on light is already very strong in the optimized 6-layer multilayer structure. The transmission time of light in the upper part of the multilayer will be longer and the oscillation will be stronger, and there will be higher energy loss. As shown in Figs. 10(c) and 10(d), the absorption performance of the optimized 6-layer multilayer structure is already pretty good, which can be compared with the unoptimized 10-layer multilayer structure.

Based on the comparison and analyses above, for the 600-nm thick alternating structure of ITO and SiO_2 multilayers, considering the trade-off between absorption effect and structural complexity, the 6-layer structure optimized by EGA is relatively ideal under the given conditions. This optimized structure achieves near-perfect absorption with large absorption bandwidth and greatly reduces the complexity of the fabrication process.

V. EGA Optimization of ENZ Multilayers With Fixed Number of Layers

The optimization process described above is for an ENZ multilayer with a fixed total thickness. In this section, the absorption performance optimization of ENZ multilayer structure with different thicknesses but fixed number of layers is discussed. The absorption performance of periodic ENZ multilayers with gradually increasing layers is optimized in the set scenario.

The unoptimized structures adopt the periodic alternating pattern of ITO and SiO_2 [23], with each layer thickness of 75 nm, and the total number of layers is successively increased

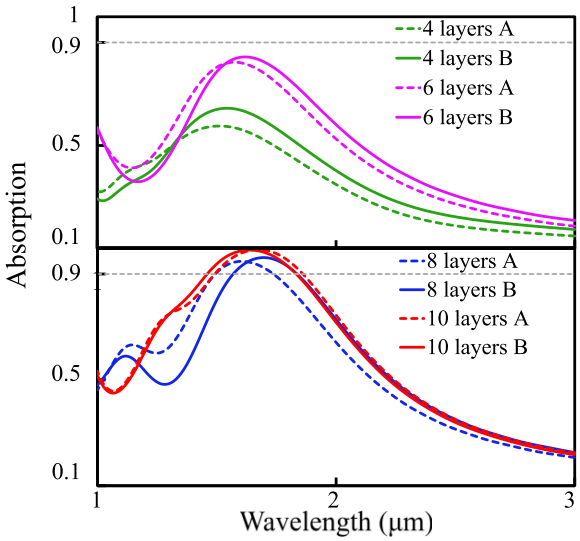

Fig. 11. The absorption characteristics of 4, 6, 8, and 10 layers before (labeled A) and after (labeled B) optimization when the total thickness is increased.

by two layers (one pair). Obviously, the absorption effect is gradually improved with the increase of thickness, as shown by the lines labeled A in Fig. 11. Based on the initial structures of these groups, EGA is used to optimize the absorption effect. The optimization results are shown as the lines labeled B in Fig. 11. When there is fewer number of layers, the EGA optimization has a greater impact on improving the absorption characteristics. In these cases, the variation in thickness of each layer greatly affects the total absorption. After optimization, the reduction in the reflected power as a consequence of reducing the mismatch between the structure and free space leads to more increase of the absorption. With the increase of the number of layers, the optimization margin of peak value and bandwidth gradually decreases. That is to say, when the total thickness increases, the interaction between layers will decrease. The increase of the total thickness plays a major role in improving the absorption, while the improvement of the absorption by EGA is not significant. This discussion can be used as a guide to achieve the absorption performance of thicker structures with smaller footprints. It is beneficial to reduce the total thickness of the material, which has a good application prospect in optical integration. As can be seen from the figures, with the increase in the number of layers, the optimization margins of peak absorption and absorption bandwidth in both Section IV and Section V present a downward trend.

VI. Conclusion

Based on the absorption characteristics of the alternating ITO and SiO_2 ENZ multilayer structure, this work optimizes the absorption performance of the structure such that it is close to a perfect absorption. An optimization algorithm EGA is proposed, which has better searching ability and convergence ability than the conventional GA. In the design process, the absorption of the multilayer system is evaluated and calculated by TMM, and the peak absorption and bandwidth of the ENZ multilayers are optimized using EGA. The optimized results break the limitation of the periodicity of traditional ENZ multilayers and form the non-periodicity structures. In the case of the 6-layer structure with a total thickness of 600 nm, EGA can optimize the peak value from 0.91 to 0.95. Additionally, the absorption bandwidth is optimized from 120 nm to 227 nm, which is enhanced more than 180%. The optimized 6-layer structure can achieve the absorption effect of a periodic 8-layer structure with the same thickness. EGA can help find an optimal structure with maximum peak absorption and absorption bandwidth in the given conditions. The absorption effect of the optimized structure is on par with that of a more complex structure with the same total thickness. It is also comparable to the absorption effect of a structure with the same number of layers but thicker total thickness.

This proposed optimization method is of versatility and can also be used to optimize other multilayer systems and complex structure designs for various purposes, such as the optimization of heat insulation performance, light transmission performance and reflection performance, etc. It is proven effective in reducing the structural footprint for optical integration and simplifying the fabrication process. From the examples presented in this work, the optimal peak absorption stabilizes around the communication wavelength, which has a great application prospect in modern communication systems and devices such as optical modulators, switches, filters and solar cells.

References

[1] A. Alù, M. G. Silveirinha, A. Salandrino, and N. Engheta, "Epsilon-near-zero metamaterials and electromagnetic sources: Tailoring the radiation phase pattern," *Phys. Rev. B*, vol. 75, no. 15, Apr. 2007, Art. no. 155410.

[2] S. Campione, D. de Ceglia, M. A. Vincenti, M. Scalora, and F. Capolino, "Electric field enhancement in ε-near-zero slabs under TM-polarized oblique incidence," *Phys. Rev. B*, vol. 87, no. 3, Jan. 2013, Art. no. 035120.

[3] S. Vassant, J.-P. Hugonin, F. Marquier, and J.-J. Greffet, "Berreman mode and epsilon near zero mode," *Opt. Exp.*, vol. 20, no. 21, pp. 23971–23977, Oct. 2012.

[4] S. Benis, N. Munera, E. W. Van Stryland, and D. J. Hagan, "Enhanced nonlinear phase-shift in epsilon-near-zero materials: The effect of group and phase velocity," in *Proc. Conf. Lasers Electro-Opt. Pacific Rim*, 2020, pp. 1–3.

[5] S. Enoch, G. Tayeb, P. Sabouroux, N. Guérin, and P. Vincent, "A metamaterial for directive emission," *Phys. Rev. Lett.*, vol. 89, no. 21, Nov. 2002, Art. no. 213902.

[6] A. Alù and N. Engheta, "Dielectric sensing in ε-near-zero narrow waveguide channels," *Phys. Rev. B*, vol. 78, no. 4, Jul. 2008, Art. no. 045102.

[7] M. Silveirinha and N. Engheta, "Tunneling of electromagnetic energy through subwavelength channels and bends using ε-Near-Zero materials," *Phys. Rev. Lett.*, vol. 97, no. 15, Oct. 2006, Art. no. 157403.

[8] M. G. Silveirinha and N. Engheta, "Theory of supercoupling, squeezing wave energy, and field confinement in narrow channels and tight bends using ε-near-zero metamaterials," *Phys. Rev. B*, vol. 76, no. 24, Dec. 2007, Art. no. 245109.

[9] N. Engheta, "Pursuing near-zero response," *Science*, vol. 340, no. 6130, pp. 286–287, Apr. 2013.

[10] X. Niu, X. Hu, Y. Xu, H. Yang, and Q. Gong, "Ultrafast all-optical polarization switching based on composite metasurfaces with gratings and an epsilon-near-zero film," *Adv. Photon. Res.*, vol. 2, no. 4, Apr. 2021, Art. no. 2000167.

[11] J. Bohn *et al.*, "All-optical switching of an epsilon-near-zero plasmon resonance in indium tin oxide," *Nat. Commun.*, vol. 12, no. 1, Dec. 2021, Art. no. 1017.

[12] Y. Yang *et al.*, "Femtosecond optical polarization switching using a cadmium oxide-based perfect absorber," *Nat. Photon.*, vol. 11, no. 6, pp. 390–395, Jun. 2017.

[13] C. Della Giovampaola and N. Engheta, "Plasmonics without negative dielectrics," *Phys. Rev. B*, vol. 93, no. 19, May 2016, Art. no. 195152.

[14] B. Edwards, A. Alù, M. E. Young, M. Silveirinha, and N. Engheta, "Experimental verification of epsilon-near-zero metamaterial coupling and energy squeezing using a microwave waveguide," *Phys. Rev. Lett.*, vol. 100, no. 3, Jan. 2008, Art. no. 033903.

[15] G. Subramania, A. J. Fischer, and T. S. Luk, "Optical properties of metal-dielectric based epsilon near zero metamaterials," *Appl. Phys. Lett.*, vol. 101, no. 24, Dec. 2012, Art. no. 241107.

[16] C. Argyropoulos, P.-Y. Chen, G. D'Aguanno, N. Engheta, and A. Alù, "Boosting optical nonlinearities in ε-near-zero plasmonic channels," *Phys. Rev. B*, vol. 85, no. 4, Jan. 2012, Art. no. 045129.

[17] S. Suresh, O. Reshef, M. Z. Alam, J. Upham, M. Karimi, and R. W. Boyd, "Enhanced nonlinear optical responses of layered Epsilon-near-zero metamaterials at visible frequencies," *ACS Photon.*, vol. 8, no. 1, pp. 125–129, Jan. 2021.

[18] M. A. Vincenti, D. de Ceglia, and M. Scalora, "ENZ materials and anisotropy: Enhancing nonlinear optical interactions at the nanoscale," *Opt. Exp.*, vol. 28, no. 21, pp. 31180–31196, Oct. 2020.

[19] Z. T. Xie, J. Wu, H. Y. Fu, and Q. Li, "Tunable electro- and all-optical switch based on epsilon-near-zero metasurface," *IEEE Photon. J.,* vol. 12, no. 4, Aug. 2020, Art no. 4501510.

[20] M. Habib, D. Briukhanova, N. Das, B. C. Yildiz, and H. Caglayan, "Controlling the plasmon resonance via epsilon-near-zero multilayer metamaterials," *Nanophotonics*, vol. 9, no. 11, pp. 3637–3644, Aug. 2020.

[21] D. Felbacq and G. Bouchitté, "Homogenization of a set of parallel fibres," *Waves Random Media*, vol. 7, no. 2, pp. 245–256, Apr. 1997.

[22] M. Koivurova, T. Hakala, J. Turunen, A. T. Friberg, M. Ornigotti, and H. Caglayan, "Metamaterials designed for enhanced ENZ properties," *New J. Phys.*, vol. 22, no. 9, Sep. 2020, Art. no. 093054.

[23] E. M. Smith *et al.*, "Epsilon-near-zero thin-film metamaterials for wideband near-perfect light absorption," *Opt. Mater. Exp.*, vol. 10, no. 10, pp. 2439–2446, Oct. 2020.

[24] J. Park, J.-H. Kang, X. Liu, and M. L. Brongersma, "Electrically tunable epsilon-near-zero (ENZ) metafilm absorbers," *Sci. Rep.*, vol. 5, no. 1, Dec. 2015, Art. no. 15754.

[25] J. Yoon, M. Zhou, M. A. Badsha, T. Y. Kim, Y. C. Jun, and C. K. Hwangbo, "Broadband epsilon-near-zero perfect absorption in the near-infrared," *Sci. Rep.*, vol. 5, no. 1, Oct. 2015, Art. no. 12788.

[26] Y. Sha, J. Wu, Z. T. Xie, H. Y. Fu, and Q. Li, "Comparison study of multi-slot designs in epsilon-near-zero waveguide-based electro-optical modulators," *IEEE Photon. J.*, vol. 13, no. 3, Jun. 2021, Art no. 4800412.

[27] A. R. Rashed, B. C. Yildiz, S. R. Ayyagari, and H. Caglayan, "Hot electron dynamics in ultrafast multilayer epsilon-near-zero metamaterials," *Phys. Rev. B*, vol. 101, no. 16, Apr. 2020, Art. no. 165301.

[28] A. Naldoni *et al.*, "Solar-energy harvesting: Broadband hot-electron collection for solar water splitting with plasmonic titanium nitride (advanced optical materials 15/2017)," *Adv. Opt. Mater.*, vol. 5, no. 15, Aug. 2017, Art. no. 1601031.

[29] M. G. Krishna, R. G. Biswas, and A. K. Bhattacharya, "On the effects of optical constants and physical parameters on the emittance of thin-film selective emitters for thermophotovoltaic applications," *J. Phys. D. Appl. Phys.*, vol. 30, no. 8, pp. 1167–1174, Apr. 1997.

[30] Q. Fu, T. He, J. L. Li, and G. W. Yang, "Surface effect on electronic and optical properties of $Bi_2Ti_2O_7$ nanowires for visible light photocatalysis," *J. Appl. Phys.*, vol. 111, no. 12, Jun. 2012, Art. no. 124306.

[31] W.-B. Liao, C.-C. Lee, Y.-C. Chang, W.-H. Cho, H.-P. Chen, and C.-C. Kuo, "Admittance analysis of broadband omnidirectional near-perfect absorber in epsilon-near-zero mode," *Appl. Opt.*, vol. 59, no. 32, pp. 10138–10142, Nov. 2020.

[32] X. Niu, X. Hu, C. Lu, Y. Sheng, H. Yang, and Q. Gong, "Broadband dispersive free, large, and ultrafast nonlinear material platforms for photonics," *Nanophotonics*, vol. 9, no. 15, pp. 4609–4618, Oct. 2020.

[33] Z. Yu, Z. Yang, Y. Wang, H. Si, and G. Zhao, "Optimized cloaks made of near-zero materials for different-sized concealed targets," *Sci. Rep.*, vol. 8, no. 1, Dec. 2018, Art. no. 16739.

[34] R. Sabri, A. Forouzmand, and H. Mosallaei, "Genetically optimized dual-wavelength all-dielectric metasurface based on double-layer epsilon-near-zero indium-tin-oxide films," *J. Appl. Phys.*, vol. 128, no. 22, Dec. 2020, Art. no. 223101.

[35] X. Niu, X. Hu, S. Chu, and Q. Gong, "Epsilon-near-zero photonics: A new platform for integrated devices," *Adv. Opt. Mater.*, vol. 6, no. 10, May 2018, Art. no. 1701292.

[36] R. Maas, J. Parsons, N. Engheta, and A. Polman, "Experimental realization of an epsilon-near-zero metamaterial at visible wavelengths," *Nat. Photon.*, vol. 7, no. 11, pp. 907–912, Nov. 2013.

[37] V. Caligiuri, R. Dhama, K. V. Sreekanth, G. Strangi, and A. De Luca, "Dielectric singularity in hyperbolic metamaterials: The inversion point of coexisting anisotropies," *Sci. Rep.*, vol. 6, no. 1, Apr. 2016, Art. no. 20002.

[38] R. M. Kaipurath *et al.*, "Optically induced metal-to-dielectric transition in epsilon-near-zero metamaterials," *Sci. Rep.*, vol. 6, no. 1, Sep. 2016, Art. no. 27700.

[39] A. Anopchenko, S. Gurung, L. Tao, C. Arndt, and H. W. H. Lee, "Atomic layer deposition of ultra-thin and smooth al-doped ZnO for zero-index photonics," *Mater. Res. Exp.*, vol. 5, no. 1, Jan. 2018, Art. no. 014012.

[40] Y. Xu and J. Xiao, "Design and numerical study of a compact, broadband and low-loss TE-pass polarizer using transparent conducting oxides," *Opt. Exp.*, vol. 24, no. 14, pp. 15373–15382, Jul. 2016.

[41] M. Z. Alam, I. De Leon, and R. W. Boyd, "Large optical nonlinearity of indium tin oxide in its epsilon-near-zero region," *Science,* vol. 352, no. 6287, pp. 795–797, May 2016.

[42] J. Wu, Z. T. Xie, Y. Sha, H. Y. Fu, and Q. Li, "Comparative study on epsilon-near-zero transparent conducting oxides: High-order chromatic dispersions and modeling of ultrashort pulse interactions," *Phys. Rev. A*, vol. 102, no. 5, Nov. 2020, Art. no. 053503.

[43] J. Wu, B. A. Malomed, H. Y. Fu, and Q. Li, "Self-interaction of ultrashort pulses in an epsilon-near-zero nonlinear material at the telecom wavelength," *Opt. Exp.*, vol. 27, no. 26, pp. 37298–37307, Dec. 2019.

[44] J. Wu, Z. T. Xie, Y. Sha, H. Y. Fu, and Q. Li, "Epsilon-near-zero photonics: Infinite potentials," *Photon. Res.,* vol. 9, no. 8, pp. 1616–1644, Aug. 2021.

[45] J. H. Holland, "Genetic algorithms and the optimal allocation of trials," *SIAM J. Comput.*, vol. 2, no. 2, pp. 88–105, Jun. 1973.

[46] F. Altiparmak, M. Gen, L. Lin, and T. Paksoy, "A genetic algorithm approach for multi-objective optimization of supply chain networks," *Comput. Ind. Eng.*, vol. 51, no. 1, pp. 196–215, Sep. 2006.

[47] Y. Rong, G. Zhang, Y. Chang, and Y. Huang, "Integrated optimization model of laser brazing by extreme learning machine and genetic algorithm," *Int. J. Adv. Manuf. Technol.*, vol. 87, no. 9–12, pp. 2943–2950, Dec. 2016.

[48] E. J. Solteiro Pires, J. A. Tenreiro Machado, and P. B. de Moura Oliveira, "Dynamical modelling of a genetic algorithm," *Signal Process.*, vol. 86, no. 10, pp. 2760–2770, Oct. 2006.

[49] K. Asan Mohideen, G. Saravanakumar, K. Valarmathi, D. Devaraj, and T. K. Radhakrishnan, "Real-coded genetic algorithm for system identification and tuning of a modified model reference adaptive controller for a hybrid tank system," *Appl. Math. Model.*, vol. 37, no. 6, pp. 3829–3847, Mar. 2013.

[50] Y. Huang, Z. Zhen, Y. Shen, C. Min, and G. Veronis, "Optimization of photonic nanojets generated by multilayer microcylinders with a genetic algorithm," *Opt. Exp.*, vol. 27, no. 2, pp. 1310–1325, Jan. 2019.

[51] L. Michaeli and A. Bahabad, "Genetic algorithm driven spectral shaping of supercontinuum radiation in a photonic crystal fiber," *J. Opt.*, vol. 20, no. 5, May 2018, Art. no. 055501.

[52] M. Lobet *et al.*, "Opal-Like photonic structuring of perovskite solar cells using a genetic algorithm approach," *Appl. Sci.*, vol. 10, no. 5, pp. 1783–1795, Mar. 2020.

[53] P. Yeh, *Optical Waves in Layered Media*, New York, NY, USA: Wiley, 1988.

[54] K. Deb and R. B. Agrawal, "Simulated binary crossover for continuous search space the crossover operator is believed to be the main search operator in the working of a genetic," *Complex Syst.,* vol. 9, no. 2, pp. 115–148, Nov. 1994.

[55] M. Srinivas and L. M. Patnaik, "Adaptive probabilities of crossover and mutation in genetic algorithms," *IEEE Trans. Syst. Man. Cybern.*, vol. 24, no. 4, pp. 656–667, Apr. 1994.

[56] J. W. Cleary, E. M. Smith, K. D. Leedy, G. Grzybowski, and J. Guo, "Optical and electrical properties of ultra-thin indium tin oxide nanofilms on silicon for infrared photonics," *Opt. Mater. Exp.*, vol. 8, no. 5, pp. 1231–1245, May 2018.

[57] B. Wan, S. Guo, Z. Zhou, D. Zhang, and H. Zhang, "Theoretical investigation on the properties of polarization selection and asymmetric absorption for the ITO nanowire material," *J. Opt. Soc. Amer. B*, vol. 37, no. 10, pp. 3126–3135, Oct. 2020.

[58] M. Amiri, F. Tofigh, N. Shariati, J. Lipman, and M. Abolhasan, "Wide-angle metamaterial absorber with highly insensitive absorption for TE and TM modes," *Sci. Rep.*, vol. 10, no. 1, Dec. 2020, Art. no. 13638.

[59] S. Lee and S. Kim, "Optical absorption characteristic in thin a-Si film embedded between an ultrathin metal grating and a metal reflector," *IEEE Photon. J.*, vol. 5, no. 5, Oct. 2013, Art. no. 4800610.